Journal of Membrane Science 527 (2017) 129–136

Contents lists available at ScienceDirect

Journal of Membrane Science

journal homepage: www.elsevier.com/locate/memsci

Cross-linked fibrous composite separator for high performance lithium-ion batteries with enhanced safety

Sae-Rom Park[a], Yun-Chae Jung[a], Won-Kyung Shin[a,b], Kyoung Ho Ahn[b], Chul Haeng Lee[b], Dong-Won Kim[a,*]

[a] Department of Chemical Engineering, Hanyang University, Seungdong-Gu, Seoul 04763, Republic of Korea
[b] Battery R & D, LG Chem, Yuseong-Gu, Daejeon 34122, Republic of Korea

ARTICLE INFO

Keywords:
Fibrous composite separator
Cross-linked separator
Polyacrylonitrile membrane
Silica nanoparticle
Lithium-ion battery

ABSTRACT

A cross-linked fibrous composite separator was prepared by thermal cross-linking between reactive silica nanoparticles and tri(ethylene glycol) diacrylate on a fibrous polyacrylonitrile (PAN) membrane. The cross-linked fibrous composite separator exhibited a three-dimensional and fully interconnected network structure in which the silica particles were firmly attached onto the PAN nanofibers through the chemical cross-linking. The separator showed good electrolyte wettability and excellent thermal stability at elevated temperatures. A lithium-ion cell composed of a graphite negative electrode, the cross-linked fibrous composite separator soaked with liquid electrolyte and a $LiNi_{0.6}Co_{0.6}Mn_{0.2}O_2$ positive electrode exhibited cycling performance and thermal safety superior to those of a cell prepared with a conventional polypropylene separator.

1. Introduction

High energy density lithium-ion batteries are rapidly becoming the preferred choice for powering portable electronic devices, electric vehicles and energy storage systems [1–4]. In these batteries, the separator is an essential component that prevents electronic contact between the positive and negative electrodes while allowing ionic transport through its porous structure. Microporous polyolefin separators such as polyethylene (PE) and polypropylene (PP) have been widely used in commercialized lithium-ion batteries because of their high mechanical strength and good chemical stability [5–7]. However, they have some drawbacks. Their low porosity and poor wettability by liquid electrolyte lead to increases in cell resistance, which restrict the high rate performance of lithium-ion batteries [8,9]. In addition, these polyolefin separators suffer from significant thermal shrinkage at elevated temperatures [10,11], which has raised serious safety concerns over their ability to prevent internal short circuits occurring at high temperatures. Therefore, it is desirable to develop new separators with good wettability and improved thermal stability to enable high performance lithium-ion batteries with enhanced safety. Fibrous polymer membranes have been investigated as good separator for lithium-ion batteries because of their higher porosity and good wettability by electrolyte solution, which would improve the cycling performance of lithium-ion batteries [12–18]. Among the various polymers that can be used to prepare fibrous membranes, polyacrylonitrile (PAN) is one of the most commonly studied polymer materials due to its superior properties, which include high ionic conductivity, good thermal stability and high electrolyte uptake [19–22]. It is also well known that introducing ceramic particles into a polymer separator can improve its thermal stability and wettability, leading to improved cycling performance and enhanced safety of lithium-ion batteries [23–26]. In our previous studies, we synthesized reactive SiO_2 particles with vinyl groups, which permitted surface reaction with vinyl monomers by free radical polymerization [27–32]. Vinyl-functionalized SiO_2 particles could be dispersed on the surface of fibrous PAN membrane, and a cross-linked composite gel polymer electrolyte was obtained by in situ cross-linking reaction using the electrolyte solution containing cross-linking agent in the lithium-ion cell after cell assembly [32]. Although adding SiO_2 particles was effective in improving the mechanical, thermal and electrical properties of the resulting composite gel polymer electrolyte, some of the SiO_2 particles may be detached from the fibrous PAN membrane during handling prior to cell assembly, since they were directly dispersed onto the PAN membrane without any binders. Thus, we tried to prepare the cross-linked fibrous composite separator using vinyl-functionalized SiO_2 particles, because the chemical cross-linking can firmly attach SiO_2 particles onto the fibrous polymer membrane before cell fabrication.

In the present study, vinyl-functionalized silica particles and tri(ethylene glycol) diacrylate (TEGDA) were coated onto the fibrous PAN membrane. A cross-linked fibrous composite separator was then

* Corresponding author.
E-mail address: dongwonkim@hanyang.ac.kr (D.-W. Kim).

http://dx.doi.org/10.1016/j.memsci.2017.01.015
Received 28 October 2016; Received in revised form 22 December 2016; Accepted 7 January 2017
Available online 09 January 2017
0376-7388/

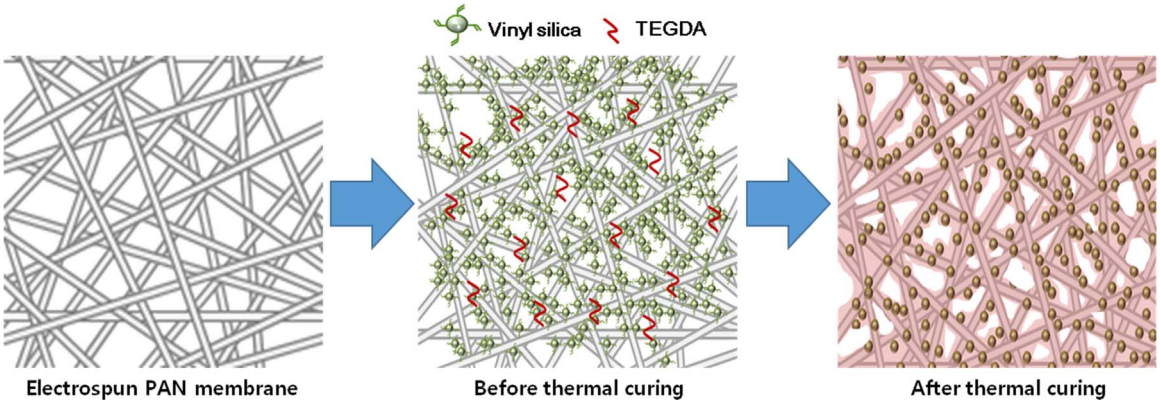

Fig. 1. Schematic illustration of the preparation of the cross-linked fibrous composite separator using a fibrous PAN membrane, vinyl SiO_2 particles and TEGDA.

prepared by inducing thermal cross-linking between reactive silica particles and TEGDA at 80 °C. It showed excellent thermal stability and high ionic conductivity when soaked with liquid electrolyte. The cross-linked fibrous composite separator was applied to fabricate the cell composed of a graphite negative electrode and a $LiNi_{0.6}Co_{0.6}Mn_{0.2}O_2$ positive electrode. The cycling performance of the lithium-ion cell was evaluated and compared to those of cells employing a conventional PP separator or a fibrous PAN membrane.

2. Experimental

2.1. Synthesis of SiO_2 particles with vinyl groups

Vinyl-functionalized SiO_2 particles were synthesized by sol–gel reaction of vinyltrimethoxysilane (VTMS, Evonik) in aqueous solution, as previously reported [27–32]. An appropriate amount of VTMS was added to double-distilled water under stirring until the VTMS droplets completely disappeared. A catalytic amount of NH_4OH in water (28 wt %, Junsei) was added to the solution, and the sol–gel reaction was allowed to proceed for 4 h at 70 °C. The resulting precipitate was centrifuged, washed several times with ethanol, and vacuum dried at 110 °C for 12 h, yielding vinyl-functionalized SiO_2 particle as a white powder.

2.2. Preparation of cross-linked fibrous composite separator

The fibrous PAN membrane was prepared by an electrospinning method [20]. A polymer solution was prepared by dissolving PAN (Mw=150,000, Sigma-Aldrich) in anhydrous N,N-dimethylformamide (DMF, Sigma-Aldrich) at a concentration of 10 wt%. For electrospinning, this solution was fed through a capillary tip by using a plastic syringe. The high voltage of 15 kV was applied to the needle, and the flow rate of the spinning solution was held at 0.8 ml h^{-1}. The distance between the tip and the rotating drum collector was 16 cm, and the metal drum was rotated at 150 rpm. Electrospun fibrous PAN membrane was collected on aluminum foil wrapped on the drum, and were dried overnight in a vacuum oven at 110 °C. The resulting fibrous PAN membrane was about 32 μm thick. The solution used to coat the fibrous PAN membrane was prepared by dispersing 5 wt% of as-prepared SiO_2 particles in isopropyl alcohol. TEGDA (Sigma-Aldrich) was added into the solution at a concentration of 10 wt% with azobisisobutyronitrile (Sigma-Aldrich, 1 wt% of TEGDA) as a thermal initiator. The as-prepared fibrous PAN membrane was immersed in this solution for 15 min, and then removed and thermally cured at 80 °C for 3 h to obtain a cross-linked fibrous composite separator, as schematically demonstrated in Fig. 1. After thermal curing, the separator was further dried in a vacuum oven at 110 °C for 24 h. The thickness of cross-linked fibrous composite separator was measured to be 35 μm. For comparison, the SiO_2-coated PE separator was also prepared by coating SiO_2 particles and poly(vinylidene fluoride-*co*-hexafluoropropylene) (P(VdF-*co*-HFP)) onto both sides of a microporous PE separator (ND 420, Asahi-Kasei Co., 20 μm). Details for preparation of the SiO_2-coated PE separator were described in our previous report [33].

2.3. Electrode preparation and cell assembly

The positive electrode was prepared by coating an N-methyl pyrrolidine (NMP)-based slurry containing $LiNi_{0.6}Co_{0.6}Mn_{0.2}O_2$, poly(-vinylidene fluoride) (PVdF), and super-P carbon (85:7.5:7.5 by weight) onto aluminum foil. Its active mass loading corresponded to a capacity of about 2.0 mAh cm^{-2}. The negative electrode was prepared similarly by coating an NMP-based slurry of mesocarbon microbeads (MCMB), PVdF, and super-P carbon (88:8:4 by weight) onto copper foil. A liquid electrolyte of consisting of 1.15 M $LiPF_6$ in ethylene carbonate (EC)/ethylmethyl carbonate (EMC)/diethyl carbonate (DEC) (3:5:2 by volume, battery grade) containing 5.0 wt% fluoroethylene carbonate (FEC) was kindly supplied by PANAX ETEC Co. Ltd. and was used as received. A CR2032-type coin cell was assembled by sandwiching a cross-linked fibrous composite separator between the graphite negative electrode and the $LiNi_{0.6}Co_{0.6}Mn_{0.2}O_2$ positive electrode and injecting the cell with liquid electrolyte. For comparison, the cells with conventional PP separator (Celgard 2400) and fibrous PAN membrane were also assembled by employing the same liquid electrolyte. All cells were assembled in an argon-filled glove box in which the moisture and oxygen content was less than 1 ppm.

2.4. Characterization and measurements

The morphologies of reactive SiO_2 particles, fibrous PAN membrane and cross-linked composite separator were examined by field emission scanning electron microscopy (FE-SEM, JEOL JSM-6330F). Fourier transform infrared (FT-IR) spectra were recorded on a JASCO 760 IR spectrometer. Thermal shrinkage of the separators was measured in terms of dimensional change after they were stored in an oven at elevated temperatures for 30 min. The mechanical properties of the separators were measured using a universal test machine (Instron 5966) in accordance with the ASTM D882 method. Porosities of the separators were measured by using mercury intrusion porosimetry (Auto Pore IV 9520, Shimadzu). To measure the ionic conductivity using each separator, a separator soaked with liquid electrolyte was sandwiched between two stainless steel electrodes. The cell was enclosed in an aluminum plastic pouch and sealed to permit testing outside of a glove box. AC impedance measurements were performed using a Zahner Electrik IM6 impedance analyzer, over the frequency range of 100100–1 MHz with the amplitude of 10 mV at 25 °C. To investigate the thermal stability of various separators integrated into lithium-ion cells, each cell was charged to 4.3 V and placed in a hot oven at 150 °C, and its open circuit voltage was then

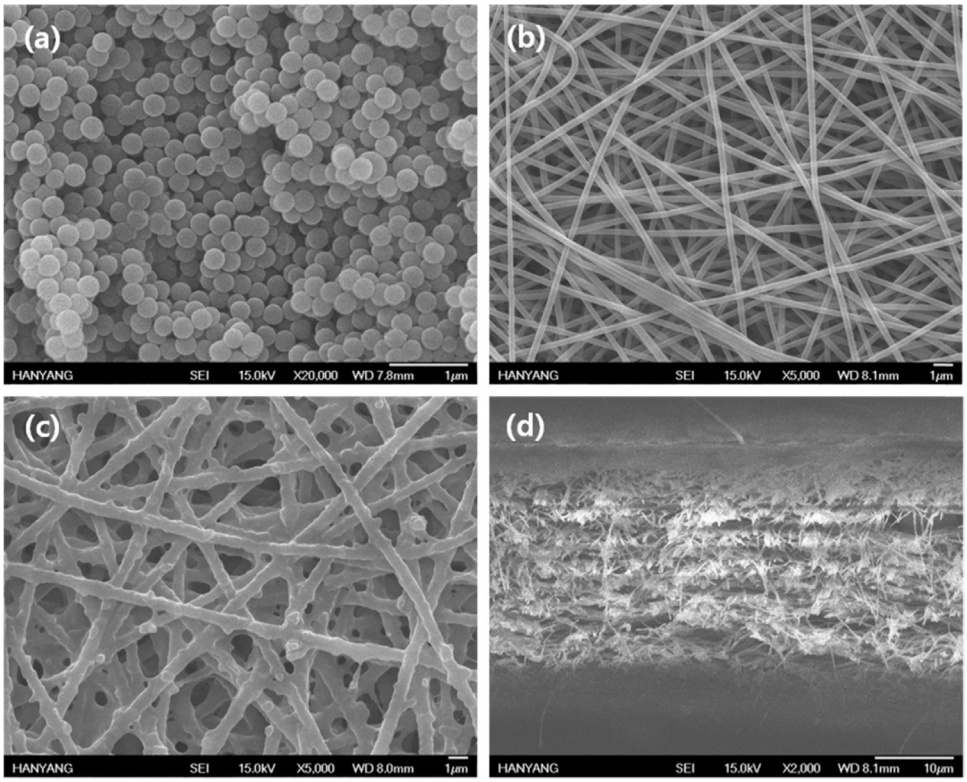

Fig. 2. FE-SEM images of (a) reactive SiO_2 particles, (b) electrospun PAN membrane, and (c) cross-linked fibrous composite separator. (d) Cross-sectional SEM image of the cross-linked fibrous composite separator.

recorded as a function of storage time [34,35]. Charge and discharge cycling tests of the lithium-ion cells were conducted at a constant current rate (0.5 C) after two conditioning cycles at a low current rate (0.1 C) over a voltage range of 2.6–4.3 V using battery testing equipment (WBCS 3000, Wonatech) at 25 °C. Various current rates were also applied to evaluate the rate capabilities of the cells.

3. Results and discussion

SEM analyses of vinyl-functionalized SiO_2 particles, the electrospun PAN membrane and the cross-linked fibrous composite separator were performed; the resulting SEM images are shown in Fig. 2. The SiO_2 particles were uniformly spherical with an average diameter of about 200 nm (Fig. 2a). The fibers in the electrospun PAN membrane were randomly arranged with an average fiber diameter of 340 nm, and included highly porous and fibrous networks in which no beads or particle aggregations were observed (Fig. 2b). As described above, the cross-linked fibrous composite separator was prepared by thermal curing between reactive SiO_2 particles and TEGDA on the fibrous PAN membrane. Because the reactive SiO_2 particles were functionalized with vinyl groups, the SiO_2 particles on the fibrous PAN membrane were able to participate in radical polymerization with TEGDA at 80 °C. As depicted in Fig. 2c, the SiO_2 particles were firmly attached onto the PAN nanofibers through the chemical cross-linking, and as a result, the diameter of the PAN/SiO_2 composite fibers was increased from 340 to 765 nm. The porosity of the cross-linked composite separator was measured to be 49.3%, which was lower than that (78.9%) of the electrospun PAN membrane. This result indicates that the increased fiber diameter brought about by cross-linking using reactive SiO_2 particles led to decreased porosity, since pore size between fibers is reduced as the fiber diameter increases. Tensile strength of cross-linked fibrous composite separator was measured to be 7.7 MPa, which was higher than that (4.5 MPa) of fibrous PAN membrane. This result suggests that the vinyl-functionalized SiO_2 particles with high mechanical strength participate in the chemical cross-linking reaction with TEGDA, thereby resulting in increase of mechanical properties. The cross-sectional morphology of cross-linked fibrous composite separator is shown in Fig. 2d. The thickness of the separator was measured to be about 35 μm by the cross-sectional image. The figure showed that the interconnected open pore structure was well remained after cross-linking between SiO_2 particles and TEGDA. In order to investigate the attachment of SiO_2 particles to the PAN membrane, both the cross-linked fibrous composite separator and the SiO_2-coated PAN membrane were immersed in liquid electrolyte and sonicated for 1 h. After drying, the mass of separators was measured to estimate the amount of SiO_2 detached from the PAN membrane. As a result, there was no change in mass of cross-linked composite separator. In contrast, 3.2% weight loss occurred in the SiO_2-coated PAN membrane. These results suggest that the SiO_2 particles were firmly attached onto the fibers in the cross-linked fibrous composite separator by chemical cross-linking reaction.

Fig. 3 presents the FT-IR spectra of fibrous PAN membrane, vinyl-functionalized SiO_2 particles and cross-linked fibrous composite separator. In the spectrum of the fibrous PAN membrane (Fig. 3a), characteristic peaks of –CN stretching vibration and C–H bending vibration were observed at 2243 and 1454 cm^{-1}, respectively [36]. For the SiO_2 particles (Fig. 3b), characteristic peaks corresponding to C=C double bonds were observed at 1410 and 1602 cm^{-1} [37], indicating the presence of the vinyl groups that permitted free radical reaction with TEGDA. The peak arising from asymmetric stretching vibrations of Si–O–Si was also observed around 1100 cm^{-1}. In the spectrum for the cross-linked fibrous composite separator (Fig. 3c), peaks corresponding to C=C double bonds could hardly be observed, indicating that the vinyl groups on the SiO_2 particles reacted with TEGDA to form the cross-linked composite polymer layer on the fibrous PAN membrane, as shown in Fig. 2c.

In order to maintain low cell resistance, the separator should be easily wetted by liquid electrolyte and should be able to absorb a large

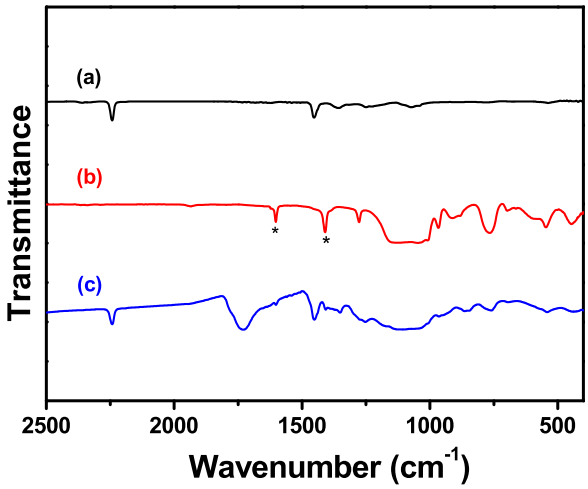

Fig. 3. FT-IR spectra of (a) electrospun PAN membrane, (b) vinyl-functionalized SiO_2 particles, and (c) cross-linked fibrous composite separator.

amount of liquid electrolyte. The wetting behavior of different separators was investigated by dropping one droplet of electrolyte solution onto each separator. As shown in Fig. 4, the PP separator was not completely wetted by the liquid electrolyte owing to its hydrophobicity and poor ability to hold organic solvents; contrastingly, both the fibrous PAN membrane and the cross-linked fibrous composite separator were immediately wetted by the liquid electrolyte. The rapid absorption and spreading of electrolyte solution on their surfaces can be attributed to the highly porous and interconnected three-dimensional fibrous network structure of the polar PAN membrane, which enabled uptake of a large amount of electrolyte solution into the porous separator. Moreover, the composite polymer layer composed of SiO_2 particles and TEGDA in the cross-linked fibrous composite separator had high affinity for the liquid electrolyte, enhancing the affinity of the separator toward liquid electrolyte. Such an enhanced wettability in the cross-linked fibrous composite separator is expected to improve the ability to retain electrolyte solution and facilitate ion transport between electrodes during cell operation. For the SiO_2-coated PE separator, the electrolyte wettability was improved as compared to PP separator (Fig. 4d). This result is due to the fact that the coating layer composed of SiO_2 particles and P(VdF-*co*-HFP) has a high affinity for the electrolyte solution. The ionic conductivities of the PP separator, fibrous PAN membrane, cross-linked fibrous composite separator and SiO_2-coated PE separator after soaking with liquid electrolyte were measured to be 4.6×10^{-4}, 1.4×10^{-3}, 2.1×10^{-3} and 7.6×10^{-4} S cm^{-1}, respectively.

Although the SiO_2-coated PE separator showed higher ionic conductivity than PP separator, it could not reach the ionic conductivity values of PAN-based separators (fibrous PAN membrane, cross-linked fibrous composite separator). The increased ionic conductivity of the PAN-based separators could be explained by their higher electrolyte uptake. It should be noted that the cross-linked fibrous composite separator soaked with liquid electrolyte exhibited slightly higher ionic conductivity than the PAN membrane soaked with same electrolyte. In the cross-linked fibrous composite separator, the liquid electrolyte can

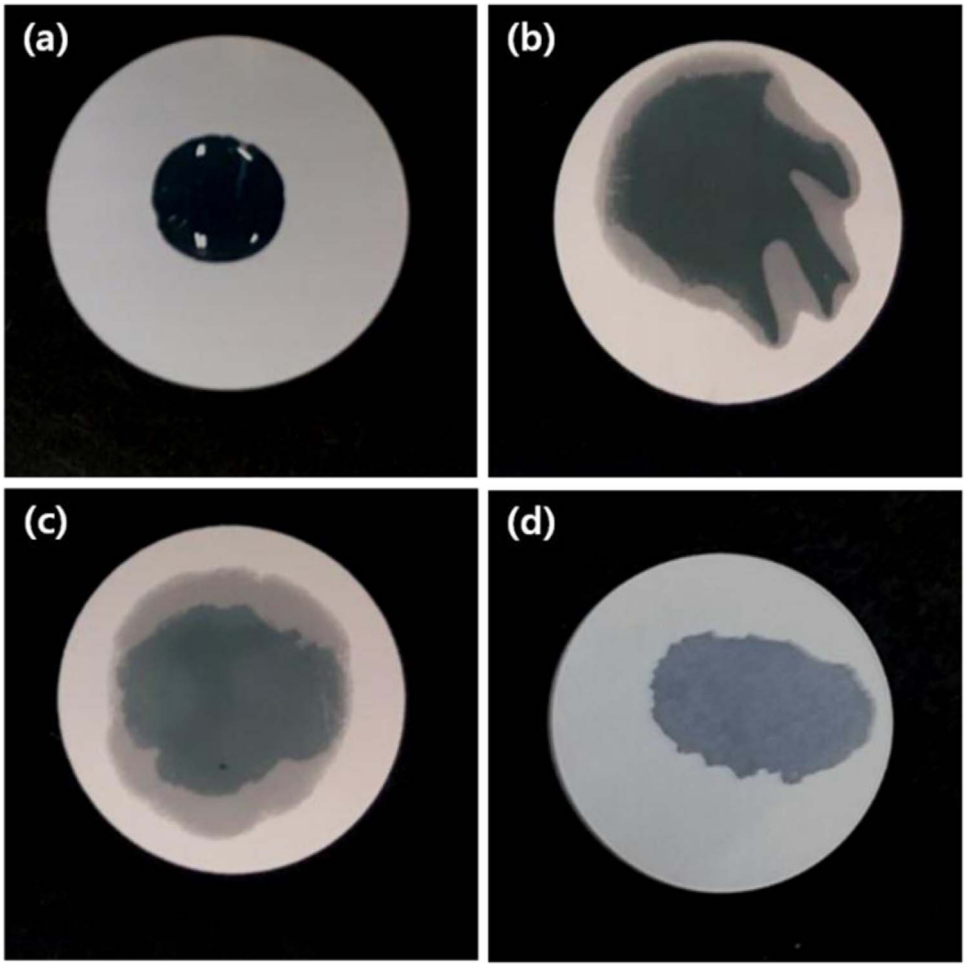

Fig. 4. Photographs of different separators after dropping of liquid electrolyte onto their surfaces: (a) PP separator, (b) fibrous PAN membrane, (c) cross-linked fibrous composite separator and (d) SiO_2-coated PE separator.

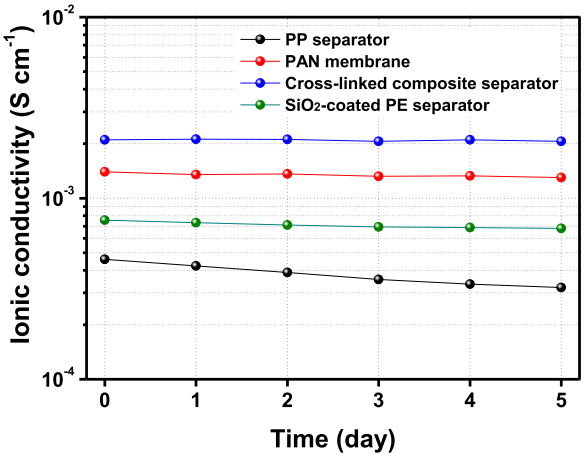

Fig. 5. Time dependence of the ionic conductivity of the different separators soaked with liquid electrolyte at room temperature.

not only be trapped in inner pores of the PAN membrane but also be retained in the hydrophilic coating layer formed by SiO_2 inorganic particles and TEGDA networks, which resulted in higher ionic conductivity of the cross-linked fibrous composite separator. These results demonstrate that the use of the cross-linked fibrous composite separator is highly effective in enhancing electrolyte wettability and reducing ionic resistance.

Fig. 5 shows time dependence of the ionic conductivity for the different separators soaked with liquid electrolyte. As discussed earlier, the PAN-based separators exhibited higher ionic conductivities over time periods measured. It is noticeable that ion conduction behavior with time was different for each separator, which can be ascribed to the difference in the retainability of liquid electrolyte in the separator. A gradual and large decrease in the ionic conductivity of the PP separator may be related to the solvent exudation upon storage due to the poor compatibility with the electrolyte solution. An almost constant value of ionic conductivity for the cross-linked fibrous composite separator for a long period of time suggests that the electrolyte solution is well retained in the porous separator, which gives no solvent exudation from the separator. Both the fibrous PAN membrane and the SiO_2-coated PE separator showed a slight decrease in ionic conductivity with time, which means that a small amount of liquid electrolyte may be exuded from the separator.

Conventional polyolefin separators usually shrink at elevated temperature, which leads to serious safety concerns. To evaluate the dimensional stability of various separators at high temperature, their thermal shrinkage behavior was examined after storing them for 30 min at 120, 130, 150, and 200 °C. As shown in Fig. 6a, the PP separator suffered from a high degree of shrinkage during the high-temperature exposure. The large shrinkage of the PP separator originated from the internal stress formed during the stretching and cooling stage of its manufacturing process. The thermal shrinkage was reduced by coating both sides of the PE separator with SiO_2 particles and polymer binder. It is considered that the ceramic coating onto both sides of the PE separator can prevent dimensional changes by thermal deformation because of the frame structure of the heat-resistant ceramic powder with polymer binder. On the other hand, both the PAN membrane and the cross-linked fibrous composite separator maintained their dimensional stability under the same thermal conditions, including exposure at 200 °C. This result is attributed to the higher thermal stability of PAN membrane compared to polyolefin separator and the incorporation of thermally resistant SiO_2 particles into the cross-linked fibrous composite separator. As a result, the cross-linked fibrous composite separator could effectively suppress thermal shrinkage, which would help to prevent internal short-circuiting at elevated temperature. To investigate the thermal safety of the cells at

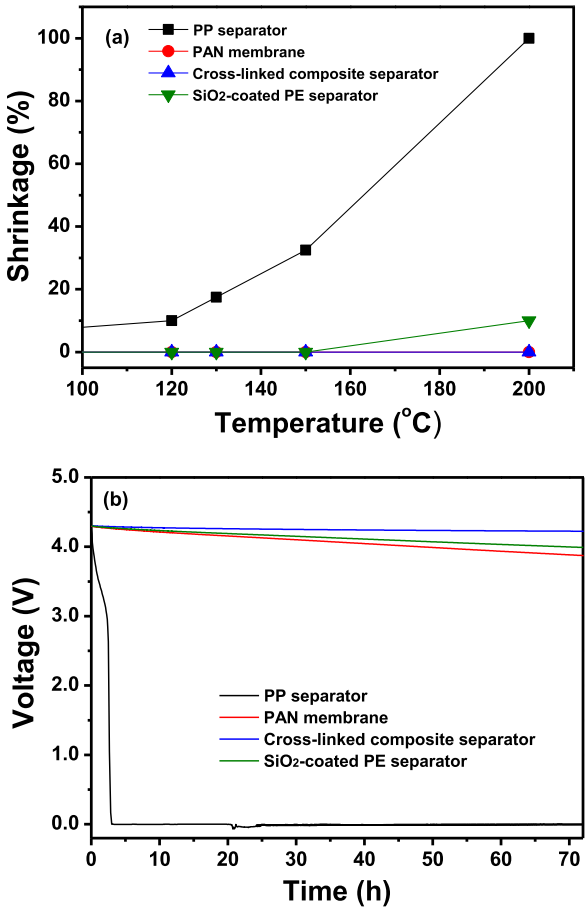

Fig. 6. Thermal stability measurements of the three different separators: (a) thermal shrinkage of different separators after high temperature exposure for 30 min, and (b) voltage variation in lithium-ion cells charged to 4.3 V as a function of storage time at 150 °C.

high temperature, the cells were charged to 4.3 V at 25 °C and the cell voltage was monitored over 72 h of storage time at 150 °C. The cell with the PP separator exhibited a large voltage drop within 3 h (Fig. 6b). This result can be ascribed to internal short-circuiting in the cell due to the dimensional change of the PP separator at 150 °C.

Although the voltage behavior of the cell with the fibrous PAN membrane was improved, it showed a gradual decrease in voltage. When the fibrous PAN membrane was soaked with electrolyte in the cell, the fine PAN fibers may become thicker by swelling and bond each other, giving rise to dimensional change of the PAN membrane in the electrolyte under high temperature environment, as previously reported [34]. It results in internal micro-short circuit and gradual decrease in voltage of the cell. Contrastingly, the cell with the cross-linked fibrous composite separator showed no voltage drop during the exposure to high temperature. These results indicate that the cross-linked fibrous composite separator containing heat-resistant SiO_2 particles can effectively suppress short-circuiting arising from the poor thermal stability of the fibrous PAN membrane in the liquid electrolyte.

The cycling performance of the lithium-ion cells assembled with different separators was evaluated. Before this testing, each cell was subjected to preconditioning cycles in the voltage range of 2.6–4.3 V at the rate of 0.1 C to induce the formation of a stable solid electrolyte interphase (SEI) layer on the electrode. The cells were then charged at 0.5 C up to the cut-off voltage of 4.3 V, and then charged at the constant voltage of 4.3 V with declining current until a final current equal to 10% of the initial charging current was obtained. The cells were then discharged to a cut-off voltage of 2.6 V at a constant current rate of 0.5 C. Fig. 7a shows the charge and discharge curves of the

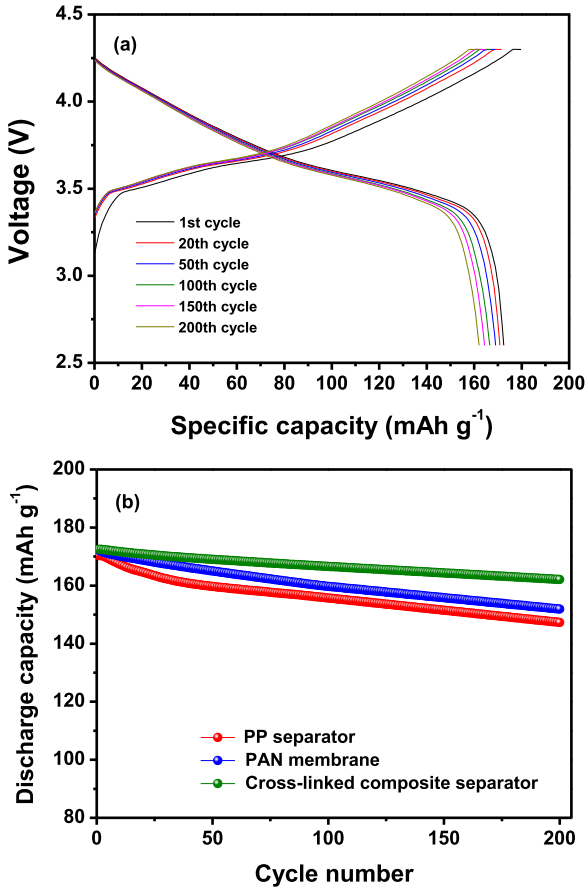

Fig. 7. (a) Charge and discharge curves of the lithium-ion cell assembled with cross-linked fibrous composite separator, and (b) discharge capacities of lithium-ion cells employing different separators (0.5 C CC and CV charge, 0.5 C CC discharge, cut-off voltage: 2.6–4.3 V, temperature: 25 °C).

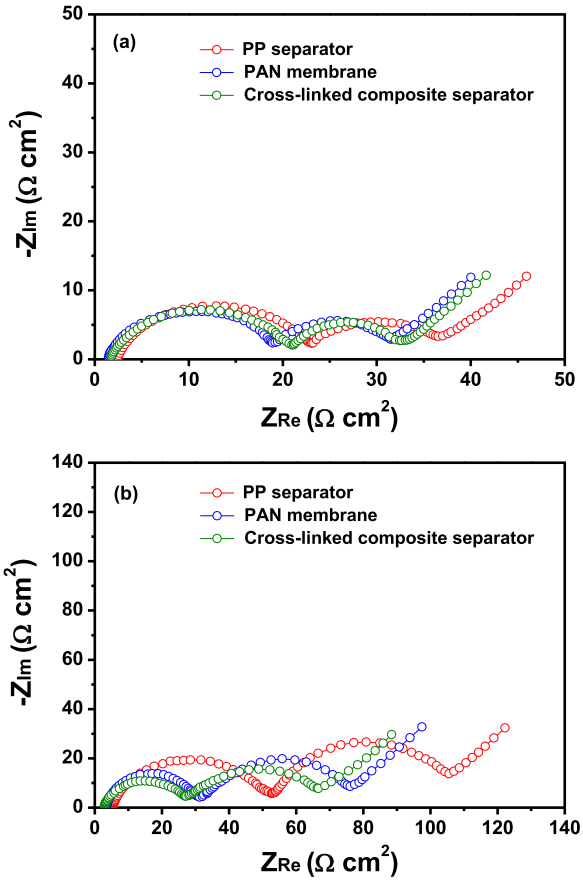

Fig. 8. AC impedance spectra of lithium-ion cells assembled with different separators, which were measured (a) after preconditioning cycles (before cycling at 0.5 C rate) and (b) after 200 cycles at 25 °C.

lithium-ion cell employing the cross-linked fibrous composite separator.

This cell initially delivered a discharge capacity of 172.5 mA h g^{-1} based on the active $LiNi_{0.6}Co_{0.2}Mn_{0.2}O_2$ material in the positive electrode. It showed stable charge and discharge curves, with a discharge capacity of 162.1 mA h g^{-1} after 200 cycles, corresponding to 94.0% of the initial discharge capacity. Fig. 7b shows the discharge capacities of lithium-ion cells assembled with different separators as a function of cycle number. As shown in figure, the cell with the cross-linked fibrous composite separator exhibited the best capacity retention among the cells with separators investigated in this study. The ability to retain electrolyte solution in the separator was enhanced by employing the cross-linked composite separator as previously discussed, which helped prevent exudation of the electrolyte solution. It resulted in facilitating the migration of lithium ions at the electrode-electrolyte interface and suppressing the increase in charge transfer resistance during the repeated cycling. Furthermore, trace amounts of acidic impurities and moisture in the electrolyte could be captured by SiO_2 particles in the cross-linked fibrous composite separator [25,38], which suppressed deleterious reactions between electrolyte solution and electrodes, resulting in more stable cycling behavior than the cell with fibrous PAN membrane.

To investigate the variations of cell impedance during cycling, the cells were subjected to AC impedance measurements before and after 200 cycles; the AC impedance spectra thus acquired are shown in Fig. 8. Each spectrum consisted of two overlapping semicircles due to the different interfacial resistance contributions: the first, in the higher frequency range, was attributed to Li^+ ion migration through the surface film on the electrodes (R_f), and the second semicircle in the middle- to low-frequency range arose from charge transfer at the electrode–electrolyte interface (R_{ct}) [39–41]. In these spectra, the high-frequency intercept at the real axis corresponds to the electrolyte resistance (R_e). Before cycling (after two preconditioning cycles), the electrolyte resistance and interfacial resistances were the highest in the cell employing the PP separator (Fig. 8a). These results can be attributed to high ionic resistance in the cell employing the PP separator, as well as to poor interfacial contacts between the PP separator and the electrodes. Contrastingly, the higher porosity and good wettability of the PAN-based separators would help to retain large amounts of the electrolyte solution in the cell, facilitating migration of lithium ions and allowing maintenance of good interfacial contacts with the electrodes. After 200 cycles (Fig. 8b), interfacial resistances increased in all cells, related to growth of the resistive surface layer on the electrode and deterioration of the interfacial contacts at the electrode. It should be noted that the cell with the cross-linked fibrous composite separator exhibited not only the lowest cell resistance but also less resistance increase after 200 cycles. As mentioned earlier, the cross-linked fibrous composite separator was highly effective in encapsulating the electrolyte solution. The presence of SiO_2 particles in the cross-linked composite separator can also stabilize the electrolyte solution by absorbing some impurities such as H_2O and HF, as discussed above, thereby improving the interfacial stability during cycling. As a result, the cell with the cross-linked fibrous composite separator exhibited the most stable cycling behavior during repeated cycling.

The rate performance of the cells assembled with different separators was evaluated at various current rates. The discharge capacities of the cells were measured during experiments in which the C rate was increased gradually every five cycles within the range of 0.2–5.0 C; the

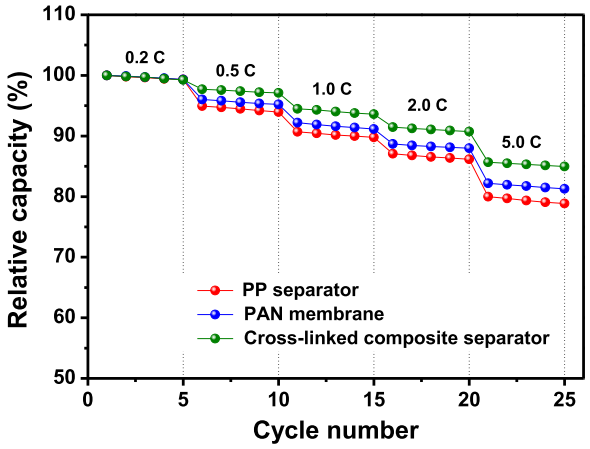

Fig. 9. Relative discharge capacities of lithium-ion cells assembled with different separators as a function of C rate at 25 °C.

results are shown in Fig. 9.

In the figure, the relative capacity is defined as the ratio of the discharge capacity at a specific C rate to the initial discharge capacity delivered at the 0.2 C rate. The discharge capacities gradually decreased due to polarization as the C rate increased. The discharge capacities of the cell employing the PP separator were the lowest among the three cells at every C rate investigated. As discussed previously, the PP separator soaked with liquid electrolyte has lower ionic conductivity, which limits the effective migration of lithium ions between the two electrodes, resulting in lower discharge capacities at high C rates. The high-rate performance was improved in the cell including the cross-linked fibrous composite separator. This result can be explained by higher ionic conductivity and lower interfacial resistances after soaking the cross-linked fibrous composite separator with liquid electrolyte.

4. Conclusions

To develop a high performance separator with enhanced thermal stability and good cycling performance, a cross-linked fibrous composite separator was prepared by free radical reaction between TEGDA and reactive silica particles on a fibrous PAN membrane. Compared with conventional PP separator, the resulting separator exhibited good wettability by liquid electrolyte, high ionic conductivity and excellent thermal stability. A lithium-ion cell employing the cross-linked fibrous composite separator showed superior cycling performance in terms of discharge capacity, cycling stability and rate capability as compared to the cell prepared with PP separator. Our results demonstrate that the cross-linked fibrous composite separator is a promising separator to improve cycling performance and thermal safety of lithium-ion batteries.

Acknowledgements

This work was supported by LG Chem. Co. Ltd. and the R & D Convergence Program of the NST (National Research Council of Science & Technology) of the Republic of Korea.

References

[1] M. Winter, R.J. Brodd, What are batteries, fuel cells, and supercapacitors?, Chem. Rev. 104 (2004) 4245–4269.
[2] A.S. Arico, P. Bruce, B. Scrosati, J.-M. Tarascon, W.V. Schalkwijk, Nanostructured materials for advanced energy conversion and storage devices, Nat. Mater. 4 (2005) 366–377.
[3] V. Etacheri, R. Marom, R. Elazari, G. Salitra, D. Aurbach, Challenges in the development of advanced Li-ion batteries: a review, Energy Environ. Sci. 4 (2011) 3243–3262.
[4] D. Larcher, J.-M. Tarascon, Towards greener and more sustainable batteries for electrical energy storage, Nat. Chem. 7 (2015) 19–29.
[5] P. Arora, Z. Zhang, Battery separators, Chem. Rev. 104 (2004) 4419–4462.
[6] S.S. Zhang, A review on the separators of liquid electrolyte Li-ion batteries, J. Power Sources 164 (2007) 351–364.
[7] J. Hassoun, S. Panero, B. Scrosati, Recent advances in liquid and polymer lithium-ion batteries, J. Mater. Chem. 17 (2007) 3668–3677.
[8] K.M. Abraham, M. Alamgir, Electrochemical science and technology: polymer Electrolytes Reinforced by Celgard Membranes, J. Electrochem. Soc. 142 (1995) 683–687.
[9] P. Yang, P. Zhang, C. Shi, L. Chen, J. Dai, J. Zhao, The functional separator coated with core-shell structured silica-poly(methyl methacrylate) sub-microspheres for lithium-ion batteries, J. Membr. Sci. 474 (2015) 148–155.
[10] I. Uchida, H. Ishikawa, M. Mohamedi, M. Umeda, AC-impedance measurements during thermal runaway process in several lithium/polymer batteries, J. Power Sources 119–121 (2003) 821–825.
[11] M.S. Wu, P.C.J. Chiang, J.C. Lin, Y.S. Jan, Correlation between electrochemical characteristics and thermal stability of advanced lithium-ion batteries in abuse tests - Short-circuit tests, Electrochim. Acta 49 (2004) 1803–1812.
[12] Y.M. Lee, J.W. Kim, N.S. Choi, J.A. Lee, W.H. Seol, J.K. Park, Novel porous separator based on PVdF and PE non-woven matrix for rechargeable lithium batteries, J. Power Sources 139 (2005) 235–241.
[13] D. Wu, C. Shi, S. Huang, X. Qiu, H. Wang, Z. Zhan, P. Zhang, J. Zhao, D. Sun, L. Lin, Electrospun nanofibers for sandwiched polyimide/poly(vinylidene fluoride) /polyimide separators with the thermal shutdown function, Electrochim. Acta 176 (2015) 727–734.
[14] J. Ding, Y. Kong, P. Li, J. Yang, Polyimide/poly(ethylene terephthalate) composite membrane by electrospinning for nonwoven separator for Lithium-ion battery, J. Electrochem. Soc. 159 (2012) A1474–A1480.
[15] X. Huang, J. Hitt, Lithium ion battery separators: development and performance characterization of a composite membrane, J. Membr. Sci. 425–426 (2013) 163–168.
[16] F. Croce, M.L. Focarete, J. Hassoun, I. Meschinia, B. Scrosati, A safe, high-rate and high-energy polymer lithium-ion battery based on gelled membranes prepared by electrospinning, Energy Environ. Sci. 4 (2011) 921–927.
[17] M. Yanilmaz, Y. Lu, M. Dirican, K. Fu, X. Zhang, Nanoparticle-on-nanofiber hybrid membrane separators for lithium-ion batteries via combining electrospraying and electrospinning techniques, J. Membr. Sci. 456 (2014) 57–65.
[18] X. Liang, Y. Yang, X. Jin, Z. Huang, F. Kang, The high performances of SiO_2/Al_2O_3-coated electrospun polyimide fibrous separator for lithium-ion battery, J. Membr. Sci. 493 (2015) 1–7.
[19] H.-S. Min, J.-M. Ko, D.-W. Kim, Preparation and characterization of porous polyacrylonitrile membranes for lithium-ion polymer batteries, J. Power Sources 119–121 (2003) 469–472.
[20] J. Zhao, S.-G. Jo, D.-W. Kim, Photovoltaic performance of dye-sensitized solar cells assembled with electrospun polyacrylonitrile/silica-based fibrous composite membranes, Electrochim. Acta 142 (2014) 261–267.
[21] M. Yanilmaz, Y. Lu, J. Zhu, X. Zhang, Silica/polyacrylonitrile hybrid nanofiber membrane separators via sol-gel and electrospinning techniques for lithium-ion batteries, J. Power Sources 313 (2016) 205–212.
[22] Q. Wang, W.-L. Song, L.-Z. Fan, Y. Song, Facile fabrication of polyacrylonitrile/alumina composite membranes based on triethylene glycol diacetate-2-propenoic acid butyl ester gel polymer electrolytes for high-voltage lithium-ion batteries, J. Membr. Sci. 486 (2015) 21–28.
[23] J.-A. Choi, S.H. Kim, D.-W. Kim, Enhancement of thermal stability and cycling performance in lithium-ion cells through the use of ceramic-coated separators, J. Power Sources 195 (2010) 6192–6196.
[24] C. Shi, P. Zhang, L. Chen, P. Yang, J. Zhao, Effect of a thin ceramic-coating layer on thermal and electrochemical properties of polyethylene separator for lithium-ion batteries, J. Power Sources 270 (2014) 547–553.
[25] C. Shi, J. Dai, X. Shen, L. Peng, C. Li, X. Wang, P. Zhang, J. Zhao, A high-temperature stable ceramic-coated separator prepared with polyimide binder/Al_2O_3 particles for lithium-ion batteries, J. Membr. Sci. 517 (2016) 91–99.
[26] H. Jeon, D. Yeon, T. Lee, J. Park, M.-H. Ryou, Y.M. Lee, A water-based Al_2O_3 ceramic coating for polyethylene-based microporous separators for lithium-ion batteries, J. Power Sources 315 (2016) 161–168.
[27] S.H. Ju, Y.-S. Lee, Y.-K. Sun, D.-W. Kim, Unique core-shell structured $SiO_2(Li^+)$ nanoparticles for high-performance composite polymer electrolytes, J. Mater. Chem. A 1 (2013) 395–401.
[28] Y.-S. Lee, J.H. Lee, J.-A. Choi, W.Y. Yoon, D.-W. Kim, Cycling characteristics of lithium powder polymer batteries assembled with composite gel polymer electrolytes and lithium powder anode, Adv. Funct. Mater. 23 (2013) 1019–1027.
[29] W.-K. Shin, Y.-S. Lee, D.-W. Kim, Study on the cycling performance of $LiNi_{0.5}Mn_{1.5}O_4$ electrodes modified by reactive SiO_2 nanoparticles, J. Mater. Chem. A 2 (2014) 6863–6869.
[30] S.-M. Park, Y.-S. Lee, D.-W. Kim, High performance lithium-ion polymer cells assembled with composite polymer electrolytes based on core-shell structured SiO_2 particles containing poly(lithium acrylate) in the shell, J. Electrochem. Soc. 162 (2015) A3071–A3076.
[31] J.-H. Yoo, W.-K. Shin, S.M. Koo, D.-W. Kim, Lithium-ion polymer cells assembled with a reactive composite separator containing vinyl-functionalized SiO_2 particles, J. Power Sources 295 (2015) 149–155.
[32] W.-K. Shin, J.H. Yoo, W. Choi, K.Y. Chung, S.S. Jang, D.-W. Kim, Cycling performance of lithium-ion polymer cells assembled with a cross-linked composite polymer electrolyte using a fibrous polyacrylonitrile membrane and vinyl-functionalized SiO_2 nanoparticles, J. Mater. Chem. A 3 (2015) 12163–12170.

[33] W.-K. Shin, D.-W. Kim, High performance ceramic-coated separators prepared with lithium ion-containing SiO_2 particles for lithium-ion batteries, J. Power Sources 226 (2013) 54–60.
[34] T.-H. Cho, M. Tanaka, H. Onishi, Y. Kondo, T. Nakamura, H. Yamazaki, S. Tanase, T. Sakai, Battery performances and thermal stability of polyacrylonitrile nano-fiber-based nonwoven separators for Li-ion battery, J. Power Sources 181 (2008) 155–160.
[35] S.-K. Kim, Y.-C. Jung, D.-H. Kim, W.-C. Shin, M. Ue, D.-W. Kim, Lithium-ion cells assembled with flexible hybrid membrane containing Li^+-conducting lithium aluminum germanium phosphate, J. Electrochem. Soc. 163 (2016) A974–A980.
[36] D. Zhang, A.B. Karki, D. Rutman, D.P. Young, A. Wang, D. Cockea, T.H. Ho, Z. Guo, Electrospun polyacrylonitrile nanocomposite fibers reinforced with Fe_3O_4 nano-particles: fabrication and property analysis, Polymer 50 (2009) 4189–4198.
[37] P. Silberzan, L. Leger, D. Ausserre, J. Benattar, Silanation of silica surfaces. A new method of constructing pure or mixed monolayers, Langmuir 7 (1991) 1647–1651.
[38] Y. Zhai, K. Xiao, J. Yu, B. Ding, Fabrication of hierarchical structured SiO_2/polyetherimide-polyurethane nanofibrous separators with high performance for lithium ion batteries, Electrochim. Acta 154 (2015) 219–226.
[39] M.D. Levi, G. Salitra, B. Markovsky, H. Teller, D. Aurbach, U. Heider, L. Heider, Solid-state electrochemical kinetics of Li-ion intercalation into $Li_{1-x}CoO_2$: simultaneous application of electroanalytical techniques SSCV, PITT, and EIS, J. Electrochem. Soc. 146 (1999) 1279–1289.
[40] S.S. Zhang, K. Xu, T.R. Jow, Electrochemical impedance study on the low temperature of Li-ion batteries, Electrochim. Acta 49 (2004) 1057–1061.
[41] T. Liu, A. Garsuch, F. Chesneau, B.L. Lucht, Surface phenomena of high energy $Li(Ni_{1/3}Co_{1/3}Mn_{1/3})O_2$/graphite cells at high temperature and high cutoff voltages, J. Power Sources 269 (2014) 920–926.